Local Geometry Analysis For Image Tampering Detection

Kais Rouis, Petra Gomez-Krämer, Mickaël Coustaty

LOCAL GEOMETRY ANALYSIS FOR IMAGE TAMPERING DETECTION

Kais Rouis, Petra Gomez-Krämer, Mickaël Coustaty

L3i, La Rochelle University, Avenue Michel Crépeau, 17042 La Rochelle, France

ABSTRACT

In this paper, we propose a compliant scheme of image hashing that is based on gradient measurement. The proposed approach relies on a local geometry variation analysis in multi-channel images. Derivative filters are used to estimate the image gradient and a suitable representation of geometric color features is introduced. A gradient norm is provided as an intermediate hash, so we compute subsequently the magnitude of the Fourier spectrum in order to provide a final hash. The aim is to preserve accurately the structural information along with smoothing operations. We conduct experiments on the CASIA-V2 database for the tampering detection task, and the UCID database to demonstrate the hash robustness. We use the metrics of true positive rate (TPR) and false positive rate (FPR) to investigate the performance of the proposed method. A comparison is carried out using two corresponding schemes; the first operates on the quaternion discrete Fourier transform (QDFT) to take into account the image color planes, and the second exploits this transform into the log-polar domain. According to the TPR results, our method is quite robust against different content-preserving operations applied on the UCID database with regard to a predefined threshold. The FPR results over CASIA-V2 further demonstrate a superior capability of the proposed approach in detecting image forgeries.

***Index Terms*—** Image hashing, tampering detection, local geometric features, image gradient.

1. INTRODUCTION

Recent technology advances have paved the way to several multimedia-based applications, especially with the spread of multimedia content in the Internet over the last decade. Furthermore, image tampering techniques have been well automated with the growth of computer vision technologies. Forgeries became in fact more realistic and harder to detect, and the produced forged copies are visually indistinguishable from the original ones. The development of efficient and accurate tampering detection techniques is indeed a crucial security issue. The easy access by novice users to a shared content makes manipulation and improper purposes more frequent. Image manipulations include several operations such as resampling the image, removing specific objects from the original version and further adding new objects to the scene from the same or different images [1].

Generally, appropriate image analysis schemes consider the human visual system (HVS) mechanisms. For instance, image object edges constitute important features [2]. However, this kind of features may be disclosed by local geometry variations. Another assumption to be expected from an appealing feature transform concerns the orientation dependency. In recent multimedia processing techniques, the perceptual characteristics, which relate to human visual system, aim to provide a compliant estimation of visual phenomena. In the same vein, tampering detection methods would process a given image taking into account the perceptual content, and preserving the consistent information of the structure of contained patterns.

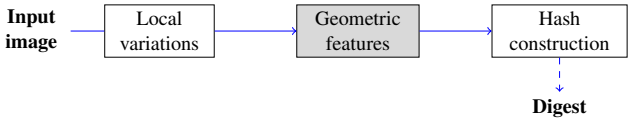

Fig. 1: Overview of proposed image hashing scheme.

Few methods have been proposed for image hashing. Some interesting approaches have been proposed based on the quaternion discrete Fourier transform (QDFT) [3, 4]. Such a transform is used to process the RGB (red, green, blue) color channels of an image. In [3], the QDFT is preceded by a log-polar transform, while QDFT-based Zernick moments are proposed in [4]. The main objective from the log-polar transform and Zernike moments is to provide a hash that is invariant to rotation as a content-preserving operation, and does not concern tampering detection issues. Another framework was introduced in [5] using the quaternion Fourier-Mellin transform to eliminate the influence of geometric distortions and a new quaternion image construction to locate tampered regions. Moreover, the authors in [6] utilized the color images using hypercomplex representations (quaternions). A different approach in [7] suggested applying a geometric correction before extracting a set of features in salient regions and statistical feature distance. These aforementioned methods evoked an explicit representation of color information involving QDFT or a geometric restoration of the processed image. The related works mainly concern the rotation invariance and/or geometric correction issues. Nonetheless, depending on the application, rotating or cropping the original image can represent a malicious attack and hence can not be considered as a content-preserving operation. The perceptual content may change after altering the geometry and the spatial position of visual patterns (hiding image content of the borders/corners). Actually, the primary issue for an image hashing is to ensure at a first level high recognition rates of tampered images and being robust to non-malicious content-preserving operations.

In our work, we propose to extract implicitly the local geometry variations in multi-channel RGB images. The main interest is to obtain convincing accuracy in recognizing tampered or similar images. The similar ones are perceptually identical to the original versions, but could be degraded with different types of noise. Fig. 1 illustrates an overview of the proposed image hashing scheme. First, a matrix is computed using first derivative Gaussian filters. This matrix corresponds to each color channel of the input image. Then, geometric features are extracted from extremum variations with regard to a structure tensor. The latter represents a suitable solution to define contours within color images. A gradient norm is finally transformed in the Fourier domain to provide the final hash (digest) over coefficient magnitudes. Our proposed approach introduces fea-

sible analysis of the image geometry variations that are derived from the concept of partial differential equations (PDEs). Our tendency is to concern the ability of exploring rich structural information using a smoothed gradient field. In comparison with the state of the art, we propose a novel approach starting from a comprehensive analytic of local color image smoothing to a provided scalar gradient norm:

- The structural information is captured by local geometric features along edges without requiring an image restoration step. The variations are measured implicitly through a subsequent transformation in the Fourier domain.
- The color information is incorporated by means of a structure tensor, so its positive eigenvalues represent variations of vector contours in a color image. Hence, we do not use quaternions contrary to several QDFT-based hashing frameworks.

The rest of the paper is organized as follows. In Section 2, we present the preliminaries about the geometry variation measurement. Section 3 describes the details of our proposed gradient-based image hashing. Experiments in Section 4 show the performance of our method based on two common image databases. Finally, some conclusions are drawn in the last section.

2. BACKGROUND AND PRELIMINARIES

Local geometric image features may be seen as preserving discontinuities in the image intensities. A convenient operation would perform a local smoothing along different directions of edges, and preserve important perceptual structures and details. Such an operation could be considered as a diffusion process over time and particularly the discretized PDEs [8, 9]. For instance, anisotropic diffusion filtering describes local image structures using a tensor T and the related divergence-based equation is commonly written in an iterative approximation:

$$\frac{\partial I_i}{\partial t} = \mathrm{div}\,(\mathrm{T}\,\nabla I_i) \;\Rightarrow\; I_{k+1} \cong I_k \;+\; \mathrm{div}(\mathrm{T}\,\nabla I_i), \tag{1}$$

where $I(I = I(t, x, y, z))$ is the image, x, y, z are the pixel coordinates and t is the diffusion time. Hence, the continuous time is replaced in a discrete function by a number of iterations. A PDE-based local smoothing of an image I is essentially defined along directions that depend themselves on the local variations of pixel intensities.

Let us consider a multi-valued image $\mathbf{I} : \Omega \to \mathbb{R}^n$ with $n = 3$ for color images, and the scalar channel $I_i : \Omega \to \mathbb{R}$: $\forall\, \mathbf{X} = (x, y) \in \Omega$, $\mathbf{I}_{(\mathbf{X})} = (I_{1(\mathbf{X})}\ I_{2(\mathbf{X})}\ ...\ I_{n(\mathbf{X})})^T$. Indeed, avoiding smoothing orthogonally the edges of $\mathbf{I}$ consists in retrieving the local geometry of contained patterns. Two directions $\theta^+_{(\mathbf{X})}$ and $\theta^-_{(\mathbf{X})}$ are defined along the maximum and minimum variations for each point $\mathbf{X} = (x, y)$, and analogous positive values $\Lambda^+_{(\mathbf{X})}$ and $\Lambda^-_{(\mathbf{X})}$ measure the local strength of an edge along $\theta^+_{(\mathbf{X})}$ and $\theta^-_{(\mathbf{X})}$ respectively. For a scalar image I_i, the local geometry is computed using the gradient ∇I_i. A smoothed gradient field $\nabla I_\sigma = \nabla I * G_\sigma$ can be then used to retrieve the local geometry, where $\Lambda^+ = \|\nabla I_\sigma\|$ corresponds to the local contour strength. Here, G_σ is a 2D-Gaussian kernel with variance σ that permits scale-space filtering. Moreover, a suited form can be expressed to represent these features in multi-valued images with a field $\mathbf{G}_{(\mathbf{X})}$ so that [10]

$$\forall \mathbf{X} \in \Omega,\ \mathbf{G}_{\mathbf{X}} = \sum_{i=1}^{n} \nabla I_{i(\mathbf{X})}\, \nabla I^T_{i(\mathbf{X})} \quad \text{where} \quad \nabla I_i = \begin{pmatrix} \frac{\partial I_i}{\partial x} \\ \\ \frac{\partial I_i}{\partial y} \end{pmatrix}. \tag{2}$$

Hence, a good estimator of the local geometry of $\mathbf{I}$ at a point $\mathbf{X}$ is a smoothed version $\mathbf{G}_\sigma = \mathbf{G} * G_\sigma$, where G_σ is the Gaussian kernel.

3. GRADIENT-BASED IMAGE HASHING

The structural information typically attracts the human perception within a visual signal. The human visual system is sensitive to the shape and orientation of an edge along with the distribution of image patterns. Accordingly, local image derivatives provide rich information and can be opted for estimating the gradient and edge directions. In our work, we employ the steerable Gaussian filters [11] to compute extremum (minimum and maximum) responses with a given scale.

On the one hand, considering only two directions may be not sufficiently accurate to describe the local geometry variations. Using a filter bank along several directions will enhance the quality of the gradient estimation such as orientations and magnitudes. On the other hand, the minimum and maximum responses form an effective estimator as it ensures implicitly the rotation invariance property and low computational costs. Besides, further enhancements can be applied to improve the edge detection for multi-channel images, taking into account the maximum and minimum variations of image intensities. In the following subsections, we will introduce the proposed local geometry analysis of multi-channel images and an adequate hashing process.

3.1. Local geometric features

Basically, Gaussian derivatives are used as a linear combination of isotropic basis filters that can be oriented at particular angles. Considering a circularly symmetric two-dimensional Gaussian function, the partial derivatives along the x-axis and y-axis are

$$\begin{cases} \frac{\partial G_\sigma(x,y)}{\partial x} = \frac{-x}{2\pi\sigma^4}\ \exp\Big(-\frac{x^2+y^2}{2\sigma^2}\Big) \\ \frac{\partial G_\sigma(x,y)}{\partial y} = \frac{-y}{2\pi\sigma^4}\ \exp\Big(-\frac{x^2+y^2}{2\sigma^2}\Big). \end{cases} \tag{3}$$

The first order Gaussian derivative $G_{\sigma,\theta}$ at an arbitrary angle can be generated by rotating the basic derivatives of isotropic Gaussian filters [11]:

$$G_{\sigma,\theta}(x, y; \sigma) = \cos(\theta)\ \frac{\partial G_\sigma(x, y)}{\partial x} \;+\; \sin(\theta)\ \frac{\partial G_\sigma(x, y)}{\partial y}. \tag{4}$$

From Eq. 4, an image channel I_i is convolved with the oriented derivative filters to obtain the corresponding responses:

$$I^\theta_i = \Big(I_i * G_{\sigma,\theta}\Big)(x, y) = \sqrt{\Big(G_{\mathbf{x}} * I_i\Big)^2 + \Big(G_{\mathbf{y}} * I_i\Big)^2}\ sin\Big(\theta + \phi\Big), \tag{5}$$

where $\phi = \arctan\Big(\frac{I_i * G_x}{I_i * G_y}\Big)$, $G_{\mathbf{x}}$ and $G_{\mathbf{y}}$ are the first partial derivatives of $G_{\sigma,\theta}$ with regard to coordinates x and y respectively [12]. Indeed, we do not consider particular angles and we obtain the maximum value I^1_i when $\theta = \pi/2 - \phi$:

$$I^1_i = \sqrt{\Big(G_{\mathbf{x}} * I_i\Big)^2 + \Big(G_{\mathbf{y}} * I_i\Big)^2}. \tag{6}$$

Furthermore, measuring the local geometry of a multi-channel image $\mathbf{I} = \Big(R, G, B\Big)$, requires the definition of the same orientations and amplitudes over all image channels I_i. This means that we have to define two orthogonal directions $\theta^+_{(\mathbf{X})}$ and $\theta^-_{(\mathbf{X})}$ that correspond to

the extremum variations at each point $\mathbf{X} = (x, y) \in \Omega$ of $\mathbf{I}$. Similar to the representation in Eq. 2, we consider a vector norm $\|d\mathbf{I}\|^2$ and a structure tensor $\mathbf{G} = \begin{pmatrix} g_{11} & g_{12} \\ g_{21} & g_{22} \end{pmatrix}$:

$$\|d\mathbf{I}\|^2 = d\mathbf{X}^T \, \mathbf{G} \, d\mathbf{X} \text{ where } \mathbf{G} = \sum_{i=1}^{n} \nabla I_i \, \nabla I_i^T, \; d\mathbf{X} = \begin{pmatrix} dx \\ dy \end{pmatrix}. \quad (7)$$

As stated in [13], $\mathbf{G}$ sums the local variations in $\mathbf{I}$ which is defined as a vector field. This tensor is further a 2×2 symmetric and positive semi-definite matrix. An elegant way to detect vector contours in a color image implies the following definition:

$$\mathbf{G} = \begin{pmatrix} R_x^2 + G_x^2 + B_x^2 & R_x R_y + G_x G_y + B_x B_y \\ R_x R_y + G_x G_y + B_x B_y & R_x^2 + G_x^2 + B_x^2 \end{pmatrix}. \quad (8)$$

Therefore, we compute the matrix G based on I_i^1, $i = \{1, 2, 3\}$ in Eq. 4 that corresponds to each color channel of $\mathbf{I^1}$ (including all the channels). The positive eigenvalues of this matrix, Λ^+ and Λ^-, give the maximum and minimum values of $\|d\mathbf{I^1}\|^2$ respectively, while the eigenvectors θ^+ and θ^- represent the orientations of these extrema. Formally, the variation measures Λ^+ and Λ^- are given by

$$\Lambda^+ = \frac{g_{11} + g_{22} + \sqrt{\Delta}}{2} \text{ and } \Lambda^- = \frac{g_{11} + g_{22} - \sqrt{\Delta}}{2}, \quad (9)$$

where $\Delta = \left(g_{11} - g_{22}\right)^2 + 4\, g_{12}^2$. High-curvature structures are hard to preserve in a smoothing-based operation. Based on Eq. 9, we propose the following norm to measure the vector-valued variations, among different choices of gradient norms:

$$f = \sqrt{\Lambda^+ + \Lambda^-}. \quad (10)$$

The above measurement represents our proposed intermediate hash and will be used in the hash construction step.

3.2. Hash construction

At this stage, f in Eq. 10 is a scalar image thanks to the defined structure (Eq. 8) which naturally incorporates the color channels along the horizontal and vertical axes. We propose to first transform this norm into the frequency domain and provide the magnitude spectrum to take advantage of the shift-invariance property.
Let us consider two gradient norms namely f_t and f_c, where f_c is a replica of f_t, but shifted by the coordinates x_0 and y_0 such that $f_c(x, y) = f_t(x - x_0, y - y_0)$. The shift property of the Fourier transform states that $F_c(u, v) = F_t(u, v)e^{-j2\pi(ux_0 + vy_0)}$. Ergo, the decomposition into the spatial-frequency space does not depend on the position of contained features. Additionally, the scalar image I_i^1 (Eq. 6) is rotationally invariant as it corresponds to an extremum response, and consequently, the obtained intermediate hash f. The idea is to ensure a robust use of this spectrum regarding the Fourier domain properties. A typical purpose is to allocate the low-frequency components from coefficients that hold the main visual information on the image structures. We compute indeed the magnitude spectrum from a selection of 5×5 coefficients after shifting the low-frequency components to the center.

Let the vector $V_0 = \{q_0^1, q_0^2, ..., q_0^N\}$ denote the coefficient magnitudes of the original image. Each vector element will be rounded to a nearest integer represented by 8 bits. As a result, the length of the generated hash is 200 bits. For the security propose, the hash will be further pseudo-randomly scrambled by using a secret key. Concretely, in our experiments, we use the *log*-spectrum V_0' to take into account the slight changes of magnitude coefficients which are sorted out to have the same order between compared vectors. Let V_1' be the vector that represents a modified version of the original image. The hashing distance is then calculated between V_0' and V_1':

$$D = \| V_0' - V_1' \|, \quad (11)$$

where $\| . \|$ is the Euclidean distance. If $D < \lambda$, then the image is authentic and perceptually similar to the original version. Otherwise, it is considered as a forged image copy. λ is a threshold that is determined empirically in the following experiments.

4. EXPERIMENTAL RESULTS AND DISCUSSION

To benchmark our proposed hashing scheme, we use two common databases in the image forensics field: CASIA-V2 [14] and UCID [15]. CASIA-V2 is a realistic open benchmark database and an extended version containing 7200 authentic images and 5123 tampered images, ranging from 320×240 to 800×600 pixels. We separate two sub-sets of tampered images: Spliced samples (CASIA_1) where the tampered region was copied from different images, and copy-move samples (CASIA_2) where the tampered region was copied from the same image. The applied manipulations in CASIA-V2 are very challenging considering that cropped regions can be processed with scaling, rotation or other distortion operations to generate a forged version. Additionally, UCID includes 1338 uncompressed original color images of 512×384 and 384×512 pixels. Similar to [3], we use the first 1000 images of this database and we adopt the same pre-processing operations. For the sake of comparison, the different images were re-scaled to 256×256 pixels and an averaging filter is applied on a 7×7 window.

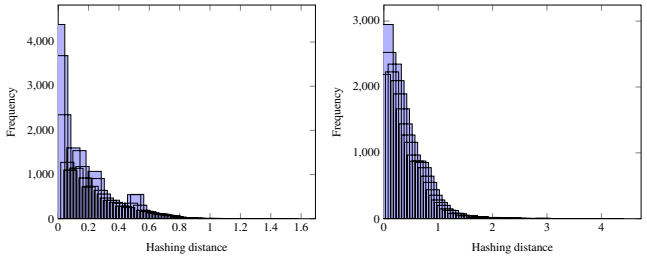

Fig. 2: Distribution of the hashing distance (D_1) of QDFT1 (left) and proposed method (right).

Diverse hashing methods use the QDFT to compute an intermediate hash. In [6], the final hash is provided by the mean of magnitudes' coefficients of image patches. For comparison, we transform an image using the QDFT and we maintain the same hash construction in our method, denoted as QDFT1. The purpose is to point out the impact of the proposed scalar norm computed over multi-channel images. We compare as well the proposed hashing scheme with the method in [3], denoted as QDFT2. The latter involves the QDFT in the log-polar domain. Fig. 2 shows the distribution of hashing distances of content-preserving operations for the UCID database. These operations were applied on each image throughout several parameters. The description and related parameters are given in Table 1. Based on this threshold, the true positive rate (TPR) and false positive rate (FPR) metrics were calculated:

$$TPR(\lambda) = \frac{n_1(D_1 < \lambda)}{N_1}, \quad FPR(\lambda) = \frac{n_2(D_2 < \lambda)}{N_2}, \quad (12)$$

where n_1 corresponds to the amount of pairs of visually identical images classified into similar images, n_2 is the amount of pairs of distinct images classified into similar images, while N_1 and N_2 denote the total number of pairs of visually similar and different images, respectively. D_1 and D_2 are the hashing distances between identical and distinct pairs, respectively. The TPR metric indicates the perceptual robustness of an image hash. From Fig. 2, a threshold $\lambda = 1$ is appropriate for the two distributions. Considering this value, QDFT1 provided in average a TPR value around 0.99. From Table 1, our method is quite robust for various content-preserving operations. Actually, we intend to prove that using a threshold which guarantees the best result of robustness for QDFT1, the performance of the proposed approach is convincing as well (an average TPR of 0.93). If we adopt the same threshold for forgery detection, the recognition rate in terms of FPR metric will be considerably better.

Table 1: TPR and hashing distance (D_1) given in average for different content-preserving operations.

Operations	Descriptions	Parameters	D_1	TPR
JPEG compression	Quality factor	10, 30, 50, 70, 90	0.1624	0.9906
Average filter	Window size	$3\times3, 5\times5, 7\times7, 9\times9, 11\times11$	0.3357	0.9656
Median filter	Window size	$3\times3, 5\times5, 7\times7, 9\times9, 11\times11$	0.5949	0.8566
Pepper & salt noise	Noise density	0.01, 0.02, 0.03, 0.05, 0.1	0.3876	0.9732
Gaussian noise	Noise variance	0.001, 0.005, 0.01, 0.02, 0.05	0.4163	0.9408
Gamma correction	Gamma value	0.75, 0.8, 0.9, 1.1, 1.25	0.5889	0.8954

Table 2: FPR and hashing distance (D_2) given in average for CASIA dataset.

	CASIA_1		CASIA_2		CASIA_All
	D_2	FPR_1	D_2	FPR_2	FPR_{all}
Proposed	1.2108	**0.4411**	2.5133	**0.1302**	**0.2730**
QDFT1	0.6905	0.7835	1.8234	0.3389	0.5364
QDFT2	—	0.7775	—	0.2964	0.5132

In our approach, we consider that rotating an original image hiding some information and generating new visual patterns within an image (such as black pixels), will change the perceptual content and thus is a malicious attack. For instance, the authors in [3] consider only the pixels inside an inscribed circle, setting to zero all remaining ones. This causes evidently a loss of information in the corners of the image and hence manipulations in these areas cannot be detected. Otherwise, if we consider the angles of 90 and 180 degrees, the average hashing distance is 0.4 and the TPR value is 0.87, which means that our hash is robust to rotation operations that do not produce perceptual content changes. To carry out tests for any rotation angles, we should consider pixels within the inscribed image circle whereas our strategy aims at detecting forgeries, being sufficiently robust, and without decreasing the security factor.

Table 2 presents the FPR metric results which indicates the discriminative capability of an image hash. The average distances D_2 of QDFT2 are not shown because it corresponds to a different range of values (normalized Hamming distance). From Table 2, one can clearly notice the superior performance of the proposed method. In contrary with the TPR metric, better results correspond to lower FPR values. Particularly, considering the second subset (CASIA_1), the compared methods obviously fail to detect copy-move forgeries (from the same image). We note that in [3], tampered images were generated from the UCID database. To the best of our knowledge, experiments in most of related works did not include all samples of CASIA-V2, and/or forged versions were generated from other datasets.

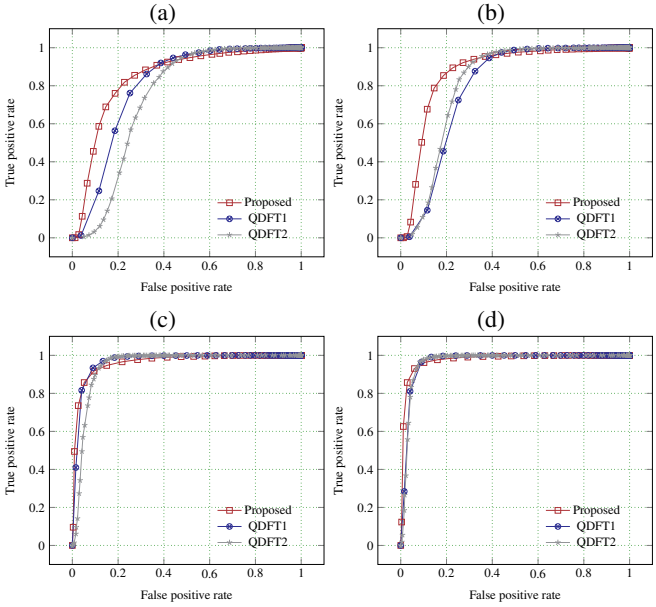

Fig. 3: Comparison through the ROC curves over CASIA_1 (first row) and CASIA_2 (second row).

The receiver operating characteristics (ROC) curves are further shown in Fig. 3 to evaluate the robustness and the authentication performances. In fact, we applied content-preserving operations (JPEG and Gaussian noise) on the images of CASIA-V2 database (same parameters in Table 1). The figures 3(a)-(b) and 3(c)-(d) concern the JPEG compression and Gaussian noise, respectively. Varying the threshold values, the ROC curves demonstrate the consistency according to both TPR and FPR metrics. Again, our approach is more robust in particular for the subset CASIA_1 and outperforms the compared schemes.

5. CONCLUSION

We described a novel method for image tampering detection where the underlying hashing process was based on the estimation of the image gradient. A convenient framework was introduced to extract local geometry variations in multi-channel images. Geometric features were extracted over extremum variations. Using these features, a gradient norm was computed and subsequently transformed in the Fourier domain. The efficiency was respectively demonstrated using two publicly available image databases. Experiments were performed to demonstrate the robustness of our provided hash against content-preserving operations, and its sensibility to different image forgeries and manipulations. The performances were compared to the use of QDFT for representing color channels in addition to a method that exploits this transform into the log-polar domain. The obtained results prove that our method is able to detect challenging image tampering operations while being robust to different types of content-preserving operations. An adaptive quantization technique is the following prospect to produce a final hash, depending on the provided spectrum distribution.

6. ACKNOWLEDGMENT

This work is financed by Region of Nouvelle-Aquitaine (SVP-IoT project, reference 2017-1R50108-00013407) and the ANR CHIST-ERA program (SPIRIT project, reference ANR-16-CHR2-0004).

7. REFERENCES

[1] Lilei Zheng, Ying Zhang, and Vrizlynn LL Thing, "A survey on image tampering and its detection in real-world photos," *Journal of Visual Communication and Image Representation*, vol. 58, pp. 380–399, 2019.

[2] Chun-Shien Lu, *Multimedia security: steganography and digital watermarking techniques for protection of intellectual property*, IGI Global, 2004.

[3] Junlin Ouyang, Gouenou Coatrieux, and Huazhong Shu, "Robust hashing for image authentication using quaternion discrete Fourier transform and log-polar transform," *Digital Signal Processing*, vol. 41, pp. 98–109, 2015.

[4] Junlin Ouyang, Xingzi Wen, Jianxun Liu, and Jinjun Chen, "Robust hashing based on quaternion Zernike moments for image authentication," *ACM Transactions on Multimedia Computing, Communications, and Applications (TOMM)*, vol. 12, no. 4s, pp. 1–13, 2016.

[5] Cai-Ping Yan, Chi-Man Pun, and Xiao-Chen Yuan, "Quaternion-based image hashing for adaptive tampering localization," *IEEE Transactions on Information Forensics and Security*, vol. 11, no. 12, pp. 2664–2677, 2016.

[6] Issam H Laradji, Lahouari Ghouti, and El-Hebri Khiari, "Perceptual hashing of color images using hypercomplex representations," in *IEEE International Conference on Image Processing*, pp. 4402–4406, 2013.

[7] Ram Kumar Karsh, Arunav Saikia, and Rabul Hussain Laskar, "Image authentication based on robust image hashing with geometric correction," *Multimedia Tools and Applications*, vol. 77, no. 19, pp. 25409–25429, 2018.

[8] Vicent Caselles, Jean-Michel Morel, Guillermo Sapiro, and Allen R Tannenbaum, "Introduction to the special issue on partial differential equations and geometry-driven diffusion in image processing and analysis," Georgia Institute of Technology, 1998.

[9] Joachim Weickert, *Anisotropic diffusion in image processing*, vol. 1, Teubner Stuttgart, 1998.

[10] Danny Barash, "Fundamental relationship between bilateral filtering, adaptive smoothing, and the nonlinear diffusion equation," *IEEE Transactions on Pattern Analysis and Machine Intelligence*, vol. 24, no. 6, pp. 844–847, 2002.

[11] William T. Freeman and Edward H Adelson, "The design and use of steerable filters," *IEEE Transactions on Pattern Analysis & Machine Intelligence*, pp. 891–906, 1991.

[12] Jun Zhang, Heng Zhao, and Jimin Liang, "Continuous rotation invariant local descriptors for texton dictionary-based texture classification," *Computer Vision and Image Understanding*, vol. 117, no. 1, pp. 56–75, 2013.

[13] Silvano Di Zenzo, "A note on the gradient of a multi-image," *Computer vision, graphics, and image processing*, vol. 33, no. 1, pp. 116–125, 1986.

[14] Jing Dong, Wei Wang, and Tieniu Tan, "Casia image tampering detection evaluation database," in *2013 IEEE China Summit and International Conference on Signal and Information Processing*. IEEE, 2013, pp. 422–426.

[15] Gerald Schaefer and Michal Stich, "UCID: An uncompressed color image database," in *Storage and Retrieval Methods and Applications for Multimedia*. International Society for Optics and Photonics, vol. 5307, pp. 472–480, 2003.